

RSC Advances



This is an *Accepted Manuscript*, which has been through the Royal Society of Chemistry peer review process and has been accepted for publication.

Accepted Manuscripts are published online shortly after acceptance, before technical editing, formatting and proof reading. Using this free service, authors can make their results available to the community, in citable form, before we publish the edited article. This *Accepted Manuscript* will be replaced by the edited, formatted and paginated article as soon as this is available.

You can find more information about *Accepted Manuscripts* in the [Information for Authors](#).

Please note that technical editing may introduce minor changes to the text and/or graphics, which may alter content. The journal's standard [Terms & Conditions](#) and the [Ethical guidelines](#) still apply. In no event shall the Royal Society of Chemistry be held responsible for any errors or omissions in this *Accepted Manuscript* or any consequences arising from the use of any information it contains.

Thiacalix[4]arene-supported heterodinuclear Ni^{II}-Ln^{III} complexes: slow magnetic relaxation behavior in dysprosium analogue

Jing-Yuan Ge, Jia-Ze Xie, Zhuang-Yu Zhao, Jing Ru, You Song, Jing-Lin Zuo*

State Key Laboratory of Coordination Chemistry, School of Chemistry and Chemical Engineering, Collaborative Innovation Center of Advanced Microstructures, Nanjing University, Nanjing 210093, P. R. China

Abstract

Three heterodinuclear complexes, [(NiL₁)Ln(L₂)(CH₃OH)]·acetone (Ln = Gd (**1**), Tb (**2**), Dy (**3**); H₃L₁ = 1,1,1-tris[(salicylideneamino)methyl]ethane), were stepwise synthesized based on a thiacalix[4]arene ligand (H₂L₂ = 5,11,17,23-tetrakis(1,1-dimethylethyl)-25,27-dihydroxy-26,28-dimethoxy thiacalix[4]arene). In **1–3**, Ni^{II} and Ln^{III} ions are doubly bridged by two phenoxo O atoms of L₁. The Ni^{II} ion, only coordinated by the L₁ ligand, features a {NiN₃O₃} coordination sphere; and Ln^{III} ion adopts a seven-coordinated {LnO₇} environment, capped by one thiacalix[4]arene ligand in a bowl-shaped conformation. Magnetic studies on all complexes reveal that ferromagnetic couplings are operative between the Ni^{II} and Ln^{III} ions. The dysprosium analogue (**3**) exhibits the field-induced single-molecule magnet (SMM) behavior under a dc-applied field of 800 Oe. Moreover, the Dy:Y (1:10) magnetically diluted sample (**3'**) shows slow magnetic relaxation at zero dc field. The results demonstrate that the stepwise synthetic method is more useful and effective than self-assemble for designing new 3d-4f heterodinuclear complexes with thiacalix[4]arene ligand or other derivatives. The introduction of the type of thiacalix[4]arene ligands into the heterodinuclear complexes renders them promising candidates for new SMMs.

* To whom correspondence should be addressed. Email: zuojl@nju.edu.cn; Fax: +86-25-83314502.
Nanjing University.

Introduction

In the past decades, single-molecule magnets (SMMs) / single-chain magnets (SCMs) have attracted much attention of chemists owing to their potential applications for high-density information storage, quantum computing, and molecular spintronics.¹ Since the first 3d-4f heterodinuclear SMM was reported in 2004,² continued efforts have been focused on the combination of 3d and 4f metal ions for new polynuclear clusters.³ Some 3d transition metal ions, especially Ni^{II} ion with a relatively large high-spin ground-state, often exhibit a large single-ion zero-field splitting.⁴ 4f ions, such as Dy^{III}, Tb^{III}, usually exhibit large ground-state spin and large intrinsic magnetic anisotropy.⁵ The ferromagnetic coupling between 3d and 4f ions often results in a high-spin ground state and may endow SMMs with a high energy barrier. A number of 3d-4f SMMs/SCMs have been reported to be ferromagnetic couplings in the literatures,⁶ such as [Dy^{III}₂Ni^{II}(Sa)₈]·(HSa)₂ (HSa = salicylic aldehyde) reported by Tang et al., of which the U_{eff} is 55.19 K.^{6c}

To the best of our knowledge, the structure of the selected ligand plays the crucial role in forming novel frameworks and tuning magnetic properties.⁷ The Schiff bases are very popular ligands serving to construct 3d-4f complexes.^{6a, 8} Take the tripodal Schiff base (1,1,1-tris[(salicylideneamino)methyl]ethane, H₃L₁) as an example, this type of ligand has two distinct bonding sites with the inner compartment (N₃O₃) to chelate 3d metal ion and the outer to accommodate 4f lanthanide ion.⁹ Yamaguchi et al. reported a Ni^{II}-complex, [Ni(H_{1.5}L₁)₂Cl·2CH₃OH], based on the tripodal ligand H₃L₁,^{9a} in which the Ni^{II} ion is chelated by a N₃O₃ group of H₃L₁. Whereafter, [(Ni^{II}L₁)Dy^{III}(hfac)₂(EtOH)] (Hhfac = hexafluoroacetylacetonate) was synthesized. The outer O atoms coordinate 4f ions to afford 3d-4f heterodinuclear complex. However, the out-of-phase signal (χ'') of [(Ni^{II}L₁)Dy^{III}(hfac)₂(EtOH)] was quite weak.^{9b} In our previous work, we have reported a series of calix[4]arene-supported lanthanide complexes, in which the Dy^{III} analogue shows obvious SMM behavior.^{10a} Calix[4]arene/thiacalix[4]arene derivatives with rigid conformation,¹⁰ are well known to be good ligand candidates for the construction of lanthanide SMMs.^{10b,10c} Usually, thiacalix[4]arene and its derivatives tend to produce clusters due to their multidentate coordination sites.¹¹ Thus, the synthesis of mononuclear or 3d-4f dinuclear complexes based on thiacalix[4]arene is still a challenging research,

which is rarely reported. To further investigate the advantages of thiacalix[4]arene in building SMMs, we aim to introduce it into 3d-4f heterodinuclear systems by the stepwise approach¹² in order to control the organization process and study their magnetic properties.

In this paper, three isomorphous Ni^{II}-Ln^{III} heterodinuclear complexes, [(NiL₁)Ln(L₂)(CH₃OH)]·acetone (Ln = Gd (**1**); Ln = Tb (**2**); Ln = Dy (**3**); H₃L₁ = 1,1,1-tris[(salicylideneamino)methyl]ethane; H₂L₂ = 5,11,17,23-tetrakis(1,1-dimethylethyl)-25,27-dihydroxy-26,28-dimethoxy thiacalix[4]arene) (Scheme 1) were successfully synthesized by treating [Ni(H_{1.5}L₁)₂Cl·2CH₃OH with Ln(acac)₃·2H₂O (Hacac = acetylacetonate) and thiacalix[4]arene ligand stepwise. Herein, the syntheses, crystal structures and magnetic properties are presented. Complex **3** shows a field-induced SMM behavior. Interestingly, a Dy:Y (molar ratio of 1:10) magnetically diluted sample (**3'**) exhibits SMM behavior at zero applied direct-current (dc) field, which conforms the important role of the dipole–dipole interaction between magnetic centers in favoring the fast quantum tunneling of magnetization (QTM) process.

Experimental Section

General Information. All chemicals and solvents were obtained and used directly from the commercial sources. Starting materials, [Ni(H_{1.5}L₁)₂Cl·2CH₃OH based on tripodal ligand 1,1,1-tris[(salicylideneamino)methyl]ethane (H₃L₁) and thiacalix[4]arene ligand (H₂L₂), were prepared according to the published literatures.^{9a,13} Elemental analyses were performed on a Elementar Vario MICRO analyzer. Infrared (IR) samples were prepared as KBr pellets, and spectra were obtained in the 400-4000 cm⁻¹ range using a Vector22 Bruker spectrophotometer. XRD patterns were obtained on a D8 ADVANCE X-ray powder diffractometer (XRPD) with Cu K α radiation ($\lambda = 1.5405 \text{ \AA}$). Inductively coupled plasma optical emission spectrometer (ICP-OES) analysis was carried out using a Perkin Elmer Optima 5300DV spectrometer. Magnetic susceptibility measurements for polycrystalline samples were performed on a Quantum Design MPMS-SQUID-VSM magnetometer in the temperature range from 2 to 300 K for direct current (dc) applied fields ranging from 0 to 70 kOe. Alternating current (ac) susceptibilities were obtained using an oscillating ac field of 2 Oe and in the frequency range 1–999 Hz. Diamagnetic corrections were calculated

using Pascal's constants,¹⁴ and an experimental correction for the diamagnetic sample holder was applied.

Crystal Structure Determination. The crystal structures were determined on a Bruker Smart Apex II CCD-based diffractometer (Mo K α radiation, $\lambda = 0.71073$ Å). The raw frame data were integrated into SHELX-format reflection files and corrected for Lorentz and polarization effects using SAINT.¹⁵ Corrections for incident and diffracted beam absorption effects were applied using SADABS supplied by Bruker.¹⁶ None of the crystals showed evidence of crystal decay during data collection. All structures were solved and refined against F^2 by the full-matrix least-squares using the SHELXL-97 program.¹⁷ The positions of the metal atoms and their first coordination spheres were located from direct method E-maps. All non-hydrogen atoms were refined with anisotropic thermal parameters, and hydrogen atoms of the organic ligands and the hydroxide anion were calculated theoretically onto the specific atoms and refined isotropically with fixed thermal factors. More details for the crystal data, data collection parameters, and refinement statistics were given in Table 1. Relevant interatomic bond distances and bond angles were listed in Table 2 and Table S1, respectively. CCDC reference numbers 1424163 (**1**), 1424164 (**2**), 1424165 (**3**).

Synthesis of [(NiL₁)Gd(L₂)(CH₃OH)]·acetone (1**).** Taking complex [Ni(H_{1.5}L₁)₂Cl·2CH₃OH (5.18 mg, 0.01 mmol) as the ligand to mixed with Et₃N (2.02 mg, 0.02 mmol) in methanol (4 mL), resulting in a yellow solution. Then Gd(acac)₃·2H₂O (9.96 mg, 0.02 mmol) was added. After stirring for 30 min, the solution appeared turbid, followed by adding H₂L₂ (14.98 mg, 0.02 mmol) and acetone (4 mL). The reaction mixture was heated at 85 °C for 3 days, and then cooled to the room temperature. Greenish yellow block-shaped crystals of **1** were obtained. Yield, 70%. Elemental analysis (%) calculated for C₇₂H₈₄GdN₃NiO₉S₄: C 58.44, H 5.72, S 8.67. Found: C, 58.69, H, 5.66, S 8.71. Selected IR frequencies (KBr pellet, cm⁻¹): 3619(w), 2960(s), 1650(s), 1634(m), 1443(vs), 1415(m), 1313(m), 1259(w), 1125(w), 1024(m), 878(w), 795(m), 593(w).

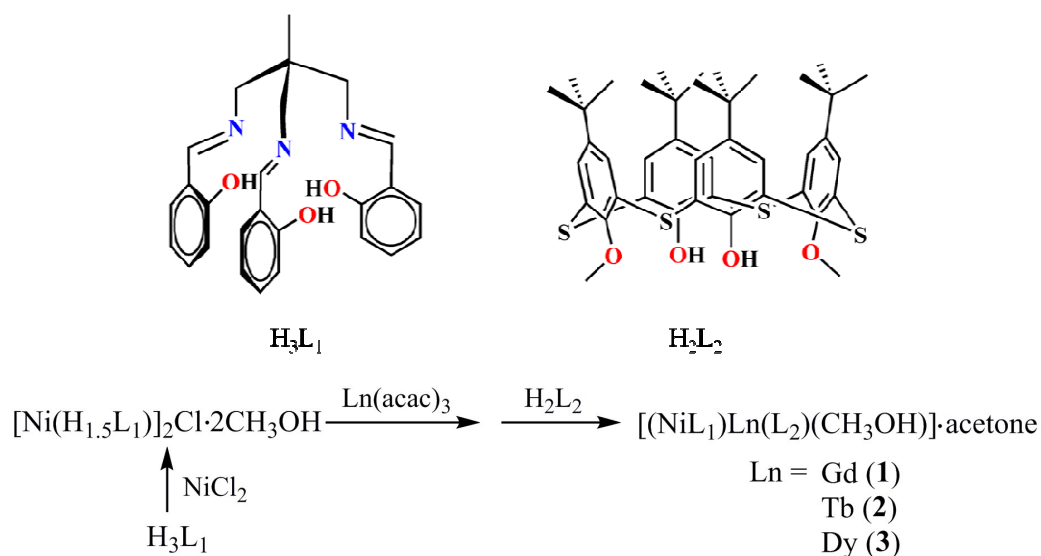
Synthesis of [(NiL₁)Tb(L₂)(CH₃OH)]·acetone (2**).** The procedure was similar to the synthesis of **1** except that Tb(acac)₃·2H₂O was used in place of Gd(acac)₃·2H₂O. Greenish yellow block-shaped crystals of **2** were obtained. Yield, 60%. Elemental analysis (%)

calculated for $C_{72}H_{84}TbN_3NiO_9S_4$: C 58.38, H 5.72, S 8.66. Found: C, 58.55, H, 5.63, S 8.60. Selected IR frequencies (KBr pellet, cm^{-1}): 3443(w), 2960(m), 1634(s), 1551(m), 1443(vs), 1415(m), 1313(m), 1259(w), 1151(w), 1024(w), 845(m), 754(m), 592(w).

Synthesis of $[(NiL_1)Dy(L_2)(CH_3OH)] \cdot acetone$ (3). The procedure was similar to the synthesis of **1** except that $Dy(acac)_3 \cdot 2H_2O$ was used in place of $Gd(acac)_3 \cdot 2H_2O$. Greenish yellow block-shaped crystals of **3** were obtained. Yield, 65%. Elemental analysis (%) calculated for $C_{72}H_{84}DyN_3NiO_9S_4$: C 58.24, H 5.70, S 8.64. Found: C, 58.58, H 5.79, S 8.55. Selected IR frequencies (KBr pellet, cm^{-1}): 3446(m), 2960(m), 1634(s), 1442(vs), 1415(m), 1314(m), 1259(m), 1122(w), 1024(w), 879(m), 754(m), 593(w).

Synthesis of $[(NiL_1)Dy_{0.071}Y_{0.929}(L_2)(CH_3OH)] \cdot acetone$ (3'). The diluted complex was prepared by following the same method as that for **1** but using $Dy(acac)_3 \cdot 2H_2O$ (0.895 mg, 0.0018 mmol) and $Y(acac)_3 \cdot 2H_2O$ (7.65 mg, 0.018 mmol) ($Dy:Y = 1:10$) instead of $Dy(acac)_3 \cdot 2H_2O$ (9.94 mg, 0.02 mmol). The final greenish yellow crystals of the doped complex were obtained with a yield of 51%. Elemental analysis (%) calculated for $C_{72}H_{84}Dy_{0.071}Y_{0.929}N_3NiO_9S_4$: C 61.05, H 5.98, S 9.05. Found: C, 59.75, H 5.76, S 8.99. IR frequencies (KBr pellet, cm^{-1}): 3444(w), 2960(m), 1650(s), 1634(m), 1443(vs), 1415(m), 1314(m), 1260(w), 1153(w), 1024(m), 878(w), 755(m), 593(w).

Results and discussion



Scheme 1. Ligands used in this work and synthetic route of **1–3**.

Synthesis and Characterizations. Complexes **1–3** were isolated by the stepwise synthetic approach in good yield (Scheme 1, Supporting information). Firstly, $[\text{Ni}(\text{H}_{1.5}\text{L}_1)]_2\text{Cl}\cdot 2\text{CH}_3\text{OH}$ and $\text{Ln}(\text{acac})_3\cdot 2\text{H}_2\text{O}$ were reacted in methanol, which became increasingly turbid after stirring. Then, H_2L_2 and acetone were added and the mixture was heated at 85 °C to obtain greenish yellow block-shaped crystals. The acac anion plays an important role in the stepwise synthetic process. It can coordinate to metal centers and occupy the coordination sites of Ln^{III} ions, but will more easily be replaced by other O-containing ligands such as thiacalix[4]arene. The stepwise synthetic approach is useful and effective for new 3d-4f heterodinuclear complexes, and it also enriches the type of metal complexes achievable based on the thiacalix[4]arenes moiety.

Crystal Structures. The X-ray crystal structure analyses reveal that **1–3** are isomorphous except for some differences in bond lengths and angles (Table 2 and Fig. S1, ESI)†. All complexes crystallize in the triclinic *Pt* space group. Each of them is a face-sharing dinuclear molecule, containing one $\text{Ni}^{\text{II}}\text{-Ln}^{\text{III}}$ heterometallic unit (Fig. 1). The Ni^{II} ion lies in an approximately octahedral $\{\text{NiN}_3\text{O}_3\}$ coordination sphere composed of three imine N atoms ($\text{Ni-N} = 2.032(4)\text{--}2.078(4)$ Å for **1**, $2.022(5)\text{--}2.093(5)$ Å for **2**, and $2.034(3)\text{--}2.087(3)$ Å for **3**, respectively) and three phenolic O atoms ($\text{Ni-O} = 2.047(3)\text{--}2.075(3)$ Å for **1**, $2.048(4)\text{--}2.066(4)$ Å for **2**, and $2.045(3)\text{--}2.077(3)$ Å for **3**, respectively) from one tripodal ligand L_1 . Every Ln^{III} ion is seven-coordinated $\{\text{LnO}_7\}$ by four O atoms of L_2 , two O atoms of L_1 , and one methanol O atom. The average Ln-O distance is 2.375, 2.366 and 2.354 Å for **1**, **2**, and **3**, respectively [in what follows, three values separated by slashes will mean a sequence in the order **1/2/3**], which are within the normal range according to previous reported values.¹⁸ It is worth noting that one of the three phenolic O atoms from L_1 is uncoordinated to a Ln^{III} ion with a long $\text{Ln}\cdots\text{O}2$ distance of 3.939/3.931/3.922 Å. Within the $\text{Ni}^{\text{II}}\text{-Ln}^{\text{III}}$ heterometallic unit, Ni^{II} and Ln^{III} ions are bridged by two O atoms (O1 and O3) from L_1 with the average Ln-O distance of 2.352/2.343/2.324 Å. The intramolecular $\text{Ni}\cdots\text{Ln}$ distance is 3.471/3.457/3.449 Å, comparable with those in the similar phenolic O atoms-bridged $\text{Ni}^{\text{II}}\text{-Ln}^{\text{III}}$ complexes.^{18,19} Subsequently, the average bond angle of Ni-O-Ln is 103.19/103.15/103.19°, and hinge angle (dihedral angle between the O-Ni-O and O-Ln-O planes) is 2.776/2.689/2.978°.

In the solid state, the acetone solvent molecule connects to the dinuclear unit *via* weak C–H \cdots O and C–H \cdots π interactions (Fig. S2a)†, and two kinds of C–H \cdots π interactions link the dinuclear units into a 1D chain with the shortest Ni \cdots Ni distance of 7.998/8.021/8.023 Å and the shortest Ln \cdots Ln distance of 9.673/9.702/9.698 Å (Fig. S2b and c)†.

Thermogravimetric analyses and X-ray powder diffraction analyses

All of the complexes are stable under ambient conditions. Thermogravimetric analyses (TGA) of **1–3** were carried out from 30 to 900 °C at a heating rate of 10 °C/min in a nitrogen atmosphere. In **1–3**, a weight loss of 4.34% (for **1**) and 4.20% (for **2**) and 4.03% (for **3**) in 30–180 °C, is assigned to the removal of one acetone molecule (calculated 3.93% for **1**, 3.92% for **2**, 3.91% for **3**, respectively). The obvious weight loss occurred from 320 to 900 °C for **1–3**, accompanying the decomposition of organic ligands, which may decompose into metallic oxides (Fig. S3)†. As shown in Fig. S4, the XRPD experimental patterns of complexes **1–3** are consistent with the simulated ones, confirming the purity of the bulk synthesized materials.

Magnetic Properties.

Static Magnetic Properties. The direct current (dc) magnetic behaviors for complexes **1–3** were measured in an applied magnetic field of 1 kOe from 2.0 K to 300 K (Fig. 2). For **1**, the $\chi_M T$ value at the room temperature is 9.41 cm³ K mol⁻¹, which is slightly higher than the expected value of 8.88 cm³ K mol⁻¹ for uncoupled Ni^{II} ($S = 1$, $g = 2$) and Gd^{III} ions ($S = 7/2$, $g = 2$). On cooling, $\chi_M T$ product remains nearly constant over the range of 300–50 K. Then, $\chi_M T$ increases sharply to a maximum value of 12.71 cm³ K mol⁻¹ at 2.5 K, close to the value of 12.38 cm³ K mol⁻¹ expected for an isolated $S = 9/2$ spin, indicating a ferromagnetic coupling between the Ni^{II} and Gd^{III} ions of **1**. Below this temperature, $\chi_M T$ drops again to a minimum value of 12.61 cm³ K mol⁻¹ at 2.0 K, which may be ascribed to the net spins in a stable state and the spin component along the external field not being changed any longer.²⁰ The experimental data between 300 and 7 K were analyzed on the basis of a simple expression derived from a spin Hamiltonian $H = -J S_{\text{Ni}} \cdot S_{\text{Gd}}$.^{18,21} The best fit parameters were $g = 2.05$ and $J = 0.80$ cm⁻¹ ($R = 2.3 \times 10^{-4}$). The positive J value is in the range ~ 0.2 – 5 cm⁻¹ for phenoxo-bridged Ni^{II}-Gd^{III} heterodinuclear complexes, which

indicates the ferromagnetic coupling between Ni^{II} and Gd^{III} ions.²² The field dependence of the magnetization for **1** was also measured at 1.9 K (Fig. 3), which is qualitatively reproduced by Brillouin curves for $S = 9/2$,²³ further confirming that the spin ground state is derived from the intramolecular ferromagnetic interaction between Ni^{II} and Gd^{III} ions. Magnetic entropy change (ΔS_m) of **1** was also calculated from the M versus H data to evaluate the magnetocaloric effect (MCE).²⁴ ΔS_m can be calculated by using the Maxwell relation $\Delta S_m(T) = \int [\partial M(T, H) / T]_H dH$ from 1.9 K to 5.0 K. The maximum value of $-\Delta S_m$ is 12.51 J kg⁻¹ K⁻¹ for a field change $\Delta H = 70$ kOe at 1.9 K (Fig. S5)†.

For **2** and **3**, the $\chi_M T$ values at the room temperature are 13.64 and 15.83 cm³ K mol⁻¹, respectively, coincide with the expected values of 12.82 and 15.17 cm³ K mol⁻¹ for uncoupled Ni^{II} ($S = 1$, $g = 2$) and Ln^{III} (Tb^{III}, $J = 6$, $g = 3/2$); Dy^{III}, $J = 15/2$, $g = 4/3$) ions (Fig. 2). As lowering temperature, the $\chi_M T$ values decrease gradually to 12.87 cm³ K mol⁻¹ at 35 K for **2**, 15.19 cm³ K mol⁻¹ at 40 K for **3**. This could be due to the thermal depopulation of the Ln^{III} ions excited Stark sublevels.²⁵ Upon further cooling, $\chi_M T$ increases sharply to a maximum value of 15.01 cm³ K mol⁻¹ at 3.0 K for **2**, 18.09 cm³ K mol⁻¹ at 3.0 K for **3**, indicating that the strong enough ferromagnetic couplings between Ni^{II} and Ln^{III} ions overwhelm the thermal depopulation of Ln^{III} ions. Below this temperature, $\chi_M T$ drops abruptly to a minimum value of 14.65 cm³ K mol⁻¹ for **2**, 17.55 cm³ K mol⁻¹ for **3**, respectively. Some additional data are also presented as the plots of M versus H in Fig. 3. As the applied magnetic field intensity increases, the magnetization increases rapidly before 10 kOe and then increases slowly to 7.75, 8.00 $N\beta$ at 70 kOe for **2** and **3**, without saturation, suggests the presence of magnetic anisotropy and/or the crystal field effects on the Ln^{III} ions.²⁶

Dynamic Magnetic Properties. Alternating current (ac) magnetic susceptibilities under $H_{ac} = 2$ Oe were performed for complexes **2** and **3** to check for any SMM behavior. For complex **2**, however, no χ'' peaks were detected even under an external dc field (Fig. S12-13)†. In the case of **3**, the obvious temperature- and frequency-dependent out-of-phase signals (χ'') were observed as typical SMM behavior. The bistability of the ground state and large intrinsic anisotropy of Dy^{III} ion are crucial to construct SMMs. At zero dc field, the

peak maxima of χ'' were observed below 2.2 K at high frequencies as χ'' versus ν plots depicted in Fig. S6†. The absence of full peaks in χ'' versus T plots indicates the existence of a fast relaxation process (Fig. S7)†, mostly resulting from QTM, which is often revealed in lanthanide SMMs.²⁷ The application of an external dc field can efficiently suppress the strong QTM and an 800 Oe field was found to be optimum for slowing down the relaxation process of **3** (Fig. S8)†. When an 800 Oe external field was introduced, the well-shaped peaks of χ'' were fully observed (Fig. 4). The resulting data were fitted to a Arrhenius law [$\tau = \tau_0 \exp(\Delta/k_B T)$] to afford the anisotropic energy barrier estimated (Δ/k_B) of 13.6 K and the pre-exponential factor $\tau_0 = 7.55 \times 10^{-6}$ s ($R = 0.9912$) (Fig. 4 inset), confirming a field-induced SMM behavior. The frequency-dependent χ'' signals exhibit gradual sweep toward the low-frequency region as the temperature was lowered to 1.9 K (Fig. 5) and Cole–Cole plots formed a symmetrically semicircular shape (Fig. 6). The generalized Debye model²⁸ allows to extract the parameter $\alpha = 0.167$ – 0.062 for temperatures between 1.9 and 5.0 K (Table S2)†, indicating a substantially single relaxation process.²⁹

In order to know the influence of intermolecular dipole-dipole interactions on the magnetic behavior, we also prepared the doped sample (**3'**) in which complex **3** was diluted by the isostructural Y^{III} analogue in a Dy/Y molar ratio of 1:10 (Fig. S9†; the exact molar ratio of Dy/Y present in the magnetically diluted sample was 0.071:0.929 extracted from ICP measurement). The dc magnetic data of **3'** were measured in detail and the well-shaped peaks of χ'' were fully observed either in the plots of χ'' versus T (Fig. 7) or χ'' versus ν (Fig. S10)† under zero dc field. The energy barrier extracted from the data modeled with the Arrhenius law is 18.1 K, with a relaxation time of 7.00×10^{-7} s ($R = 0.9965$) (Fig. 7 inset), suggesting the doped sample **3'** features SMM behavior under zero dc field. Cole–Cole plots, which show semicircular shapes within the temperature range from 1.9 to 3.5 K, are fitted to a generalized Debye model²⁸ to give values of α in the range of 0.239–0.108 (Fig. S11)†. The relatively large α values might indicate the presence of multiple relaxation processes. Interestingly, the adiabatic susceptibility (χ_s) for the diluted sample (**3'**) reduces regularly with the increase of temperature (Table S3)†,³⁰ which is different from that for **3** (Table S2)†. We think it is likely to be due to the diamagnetic dilution that remarkably weakened the dipole-dipole interaction between the molecules.^{25,31} Further analysis is needed to investigate the relaxation paths in **3'**.

It is worth mentioning that the dynamic magnetic behavior of **3** is different from that of one related Ni^{II}-Dy^{III} dinuclear complex, [(NiL₁)Dy(hfac)₂(EtOH)] (Hhfac = hexafluoroacetylacetone).^{9b} [(NiL₁)Dy(hfac)₂(EtOH)] is also ferromagnetically coupled and shows a slow magnetic relaxation. However, the χ'' signal is quite weak and SMM behavior cannot be drawn effectively. Meanwhile, complex **3** exhibits strong temperature- and frequency-dependence, a characteristic behavior of SMM. In these two complexes, the octahedral coordination spheres of Ni^{II} ions are the same, but Dy^{III} ions adopt two significantly different coordination geometries. Further analyses of the geometries of Dy^{III} ions are determined by SHAPE 2.1 software. For [(NiL₁)Dy(hfac)₂(EtOH)], Dy^{III} ion is eight-coordinated and lies in a triangular dodecahedron (*D*_{2d}) symmetry, while Dy^{III} ion is seven-coordinated and the coordination symmetry is close to pentagonal bipyramid (*D*_{5h}) in **3** (Table S4)†. Introduction the thiacalix[4]arene ligand alters the structure and crystal field resulting in significantly different magnetic properties. Further compared to another similar Ni^{II}-Dy^{III} complex, [Ni(CH₃CN)(H₂O)(valpn)Ln(NO₃)(H₂O)₃] (H₂valpn = 1,3-propanediylbis(2-iminomethylene-6-methoxy-phenol))²², in which the maximum χ'' value is seen above 2 K only for the highest frequency 1490 Hz under 1000 Oe dc field, we can conclude the thiacalix[4]arene derivatives, which have large steric hindrance and rigid conformation which afford a “protective” sheath and weaken intermolecular f-f interactions,^{10a} are good ligand candidates for the construction of lanthanide-based SMMs.

Conclusions

In summary, three thiacalix[4]arene-supported Ni^{II}-Ln^{III} heterodinuclear complexes were successfully synthesized. All the complexes feature diphenoxo-bridged Ni^{II}-Ln^{III} dinuclear species. Detailed magnetic studies reveal weak ferromagnetic coupling between Ni^{II} and Ln^{III} ions. Complex **3** exhibits a field-induced slow magnetic relaxation with an effective thermal barrier of 13.8 K and a relaxation time of 7.55×10^{-6} s, which is typical for SMMs. Furthermore, the magnetic relaxation behavior of diluted sample with a molar ratio Dy/Y of 1:10, reveals magnetic dilution can efficiently reduce the QTM incurred by intermolecular dipolar interactions. The stepwise synthetic strategy is an efficient approach to construct new 3d-4f heterodinuclear complexes with thiacalix[4]arene and other types of tetradentate ligands (such as porphyrins and phthalocyanines), which is of interest for synthetic

chemistry. Additionally, the introduction of thiacalix[4]arene ligand into the heterodinuclear complexes is useful for interesting single-molecule magnets.

Acknowledgments

This work was supported by the Major State Basic Research Development Program (2013CB922101), the National Natural Science Foundation of China (51173075 and 91433113), and the Natural Science Foundation of Jiangsu Province (BK20130054). We also thank Dr. Tian-Wei Wang for the experimental assistance in conducting magnetic measurements.

Supporting Information

Selected bond lengths and angles, TGA curves, XRPD patterns, magnetic characterizations and X-ray crystallographic files in CIF format for **1–3**. This information is available free of charge *via* the Internet at <http://www.rsc.org>.

References

- (a) F. Troiani, M. Affronte, *Chem. Soc. Rev.*, 2011, **40**, 3119. (b) R. Sessoli, H. L. Tsai, A. R. Schake, S. Wang, J. B. Vincent, K. Folting, D. Gatteschi, G. Christou, D. N. Hendrickson, *J. Am. Chem. Soc.*, 1993, **115**, 1804. (c) R. Sessoli, D. Gatteschi, A. Caneschi, M. A. Novak, *Nature*, 1993, **365**, 141. (d) K. Binnemans, *Coord. Chem. Rev.*, 2009, **109**, 4283. (e) K. S. Pedersen, J. Bendix, R. Clérac, *Chem. Commun.*, 2014, **50**, 4396. (f) T. D. Harris, M. V. Bennett, R. Clérac, J. R. Long, *J. Am. Chem. Soc.*, 2010, **132**, 3980. (g) K. Qian, X. C. Huang, C. Zhou, X. Z. You, X. Y. Wang, K. R. Dunbar, *J. Am. Chem. Soc.*, 2013, **135**, 13302. (h) M. Morimoto, H. Miyasaka, M. Yamashita, M. Irie, *J. Am. Chem. Soc.*, 2009, **131**, 9823.
- S. Osa, T. Kido, N. Matsumoto, N. Re, A. Pochaba, J. Mrozinski, *J. Am. Chem. Soc.*, 2004, **126**, 420.
- (a) L. Chen, J. Wang, J. M. Wei, W. Wernsdorfer, X. T. Chen, Y. Q. Zhang, Y. Song, Z. L. Xue, *J. Am. Chem. Soc.*, 2014, **136**, 12213. (b) Y. N. Guo, G. F. Xu, P. Gamez, L. Zhao, S. Y. Lin, R. Deng, J.-K. Tang, H. J. Zhang, *J. Am. Chem. Soc.*, 2010, **132**, 8538. (c) J. Long, R. Vallat, R. A. Ferreira, L. D. Carlos, F. A. Almeida Paz, Y. Guari, J.

- Larionova, *Chem. Commun.*, 2012, **48**, 9974. (d) J. Rinck, G. Novitchi, W. Van den Heuvel, L. Ungur, Y. Lan, W. Wernsdorfer, C. E. Anson, L. F. Chibotaru, A. K. Powell, *Angew. Chem. Int. Ed.*, 2010, **49**, 7583. (e) L. Rosado Piquer, E. C. Sañudo, *Dalton Trans.*, 2015, **44**, 8771.
- 4 (a) F. H. Zhao, H. Li, Y. X. Che, J. M. Zheng, V. Vieru, L. F. Chibotaru, F. Grandjean, G. J. Long, *Inorg. Chem.*, 2014, **53**, 9785. (b) G. Rogez, J. N. Rebilly, A. L. Barra, L. Sorace, G. Blondin, N. Kirchner, M. Duran, J. van Slageren, S. Parsons, L. Ricard, A. Marvilliers, T. Mallah, *Angew. Chem. Int. Ed.*, 2005, **44**, 1876.
- 5 (a) D. N. Woodruff, R. E. Winpenny, R. A. Layfield, *Chem. Rev.*, 2013, **113**, 5110. (b) Y. N. Guo, G. F. Xu, Y. Guo, J.-K. Tang, *Dalton Trans.*, 2011, **40**, 9953. (c) P.-H. Guo, J. Liu, Z.-H. Wu, H. Yan, Y.-C. Chen, J.-H. Jia, M.-L. Tong, *Inorg. Chem.*, 2015, **54**, 8087.
- 6 (a) E. Colacio, J. Ruiz-Sanchez, F. J. White, E. K. Brechin, *Inorg. Chem.*, 2011, **50**, 7268. (b) J.-F. Wu, L. Zhao, P. Zhang, L. Zhang, M. Guo, J.-K. Tang, *Dalton Trans.*, 2015, **44**, 11935. (c) X. L. Li, F. Y. Min, C. Wang, S. Y. Lin, Z. Liu, J.-K. Tang, *Inorg. Chem.*, 2015, **54**, 4337. (d) M. Towatari, K. Nishi, T. Fujinami, N. Matsumoto, Y. Sunatsuki, M. Kojima, N. Mochida, T. Ishida, N. Re, J. Mrozinski, *Inorg. Chem.*, 2013, **52**, 6160. (e) J.-L. Liu, J.-Y. Wu, Y.-C. Chen, V. Mereacre, A. K. Powell, L. Ungur, L. F. Chibotaru, X.-M. Chen, M.-L. Tong, *Angew. Chem. Int. Ed.*, 2014, **53**, 12966.
- 7 (a) W.-B. Sun, B. Yan, Y.-Q. Zhang, B.-W. Wang, Z.-M. Wang, J.-H. Jia, S. Gao, *Inorg. Chem. Front.*, 2014, **1**, 503. (b) L. Sorace, C. Benelli, D. Gatteschi, *Chem. Soc. Rev.*, 2011, **40**, 3092. (c) J. Liu, Y.-C. Chen, Z.-X. Jiang, J.-L. Liu, J.-H. Jia, L.-F. Wang, Q.-W. Li, M.-L. Tong, *Dalton Trans.*, 2015, **44**, 8150.
- 8 (a) X. Feng, W. Zhou, Y. Li, H. Ke, J.-K. Tang, R. Clérac, Y. Wang, Z. Su, E. Wang, *Inorg. Chem.*, 2012, **51**, 2722. (b) P. Bag, J. Goura, V. Mereacre, G. Novitchi, A. K. Powell, V. Chandrasekhar, *Dalton Trans.*, 2014, **43**, 16366. (c) M. Andruh, J.-P. Costes, C. Diaz, S. Gao, *Inorg. Chem.*, 2009, **48**, 3342. (d) H. L. C. Feltham, R. Clérac, A. K. Powell, S. Brooker, *Inorg. Chem.*, 2011, **50**, 4232.
- 9 (a) T. Yamaguchi, Y. Sunatsuki, H. Ishida, *Acta Crystallogr.*, 2008, **C64**, m156. (b) T. Yamaguchi, Y. Sunatsuki, H. Ishida, M. Kojima, H. Akashi, N. Re, N. Matsumoto, A. Pochaba, J. Mroziński, *Inorg. Chem.*, 2008, **47**, 5736. (c) T. Yamaguchi, J.-P. Costes, Y.

- Kishima, M. Kojima, Y. Sunatsuki, N. Bréfuel, J.-P. Tuchagues, L. Vendier, W. Wernsdorfer, *Inorg. Chem.*, 2010, **49**, 9125.
- 10 (a) F. Gao, L. Cui, Y. Song, Y.-Z. Li, J.-L. Zuo, *Inorg. Chem.*, 2014, **53**, 562. (b) R. Kumar, Y. O. Lee, V. Bhalla, M. Kumar, J. S. Kim, *Chem. Soc. Rev.*, 2014, **43**, 4824. (c) Y.-F. Bi, X.-T. Wang, W.-P. Liao, X.-W. Wang, R.-P. Deng, H.-J. Zhang, S. Gao, *Inorg. Chem.*, 2009, **48**, 11743. (d) R. E. Fairbairn, R. McLellan, R. D. McIntosh, M. A. Palacios, E. K. Brechin, S. J. Dalgarno, *Dalton Trans.*, 2014, **43**, 5292. (e) S. Kennedy, C. M. Beavers, S. J. Teat, S. J. Dalgarno, *CrystEngComm*, 2014, **16**, 3712. (f) P. K. Thallapally, S. J. Dalgarno, J. L. Atwood, *J. Am. Chem. Soc.*, 2006, **128**, 15060.
- 11 (a) K. Su, F. Jiang, J. Qian, L. Chen, J. Pang, S. M. Bawaked, M. Mokhtar, S. A. Al-Thabaiti, M.-C. Hong, *Inorg. Chem.*, 2015, **54**, 3183. (b) K. Su, F. Jiang, J. Qian, M. Wu, K. Xiong, Y. Gai, M.-C. Hong, *Inorg. Chem.*, 2013, **52**, 3780. (c) J.-Y. Ge, J. Ru, F. Gao, Y. Song, X.-H. Zhou, J.-L. Zuo, *Dalton Trans.*, 2015, **44**, 15481.
- 12 S. Ghosh, Y. Ida, T. Ishida, A. Ghosh, *Cryst. Growth Des.*, 2014, **14**, 2588.
- 13 H. Dvorakova, J. Lang, J. Vlach, J. Sykora, M. Cajan, M. Himl, M. Pojarova, I. Stibor, P. Lhotak, *J. Org. Chem.*, 2007, **72**, 7157.
- 14 E. A. Boudreaux, L. N. Mulay, *Theory and Application of Molecular Paramagnetism*; John Wiley & Sons: New York, 1976; p 491.
- 15 *SAINT-Plus*, version 6.02; Bruker Analytical X-ray System: Madison, WI, 1999.
- 16 G. M. Sheldrick, *SADABS an empirical absorption correction program*; Bruker Analytical X-ray Systems: Madison, WI, 1996.
- 17 G. M. Sheldrick, *Acta Crystallogr.* 2008, **A64**, 112.
- 18 X.-Y. Lu, Y.-Q. Liu, X.-W. Deng, Z.-X. Zhu, M.-X. Yao, S. Jing, *New J. Chem.*, 2015, **39**, 3467.
- 19 T. D. Pasatoiu; M. Etienne, A. M. Madalan, M. Andruh, R. Sessoli, *Dalton Trans.*, 2010, **39**, 4802.
- 20 J.-H. Wang, P.-F. Yan, G.-M. Li, J.-W. Zhang, P. Chen, M. Suda, Y. Einaga, *Inorg. Chim. Acta*, 2010, **363**, 3706.
- 21 J. P. Costes, F. Dahan, A. Dupuis, J. P. Laurent, *Inorg. Chem.*, 1997, **36**, 4284.
- 22 T. D. Pasatoiu, J. P. Sutter, A. M. Madalan, F. Z. Fellah, C. Duhayon, M. Andruh, *Inorg. Chem.*, 2011, **50**, 5890.

- 23 M. G. Alexandru, D. Visinescu, S. Shova, F. Lloret, M. Julve, M. Andruh, *Inorg. Chem.*, 2013, **52**, 11627.
- 24 (a) M. Manoli, A. Collins, S. Parsons, A. Candini, M. Evangelisti, E. K. Brechin, *J. Am. Chem. Soc.*, 2008, **130**, 11129. (b) J. Ruiz, G. Lorusso, M. Evangelisti, E. K. Brechin, S. J. A. Pope, E. Colacio, *Inorg. Chem.*, 2014, **53**, 3586. (c) J. W. Sharples, Y.-Z. Zheng, F. Tuna, E. J. L. McInnes, D. Collison, *Chem. Commun.*, 2011, **47**, 7650. (d) W. Sethi, S. Sanz, K. S. Pedersen, M. A. Sørensen, G. S. Nichol, G. Lorusso, M. Evangelisti, E. K. Brechin, S. Piligkos, *Dalton Trans.*, 2015, **44**, 10315. (e) M. Manoli, R. D. L. Johnstone, S. Parsons, M. Murrie, M. Affronte, M. Evangelisti, E. K. Brechin, *Angew. Chem. Int. Ed.*, 2007, **46**, 4456.
- 25 Y. Bi, Y.-N. Guo, L. Zhao, Y. Guo, S.-Y. Lin, S.-D. Jiang, J.-K. Tang, B.-W. Wang, S. Gao, *Chem. Eur. J.*, 2011, **17**, 12476.
- 26 J. Goura, R. Guillaume, E. Riviere, V. Chandrasekhar, *Inorg. Chem.*, 2014, **53**, 7815.
- 27 (a) G. Brunet, F. Habib, I. Korobkov, M. Murugesu, *Inorg. Chem.*, 2015, **54**, 6195. (b) E. Moreno Pineda, N. F. Chilton, F. Tuna, R. E. P. Winpenny, E. J. L. McInnes, *Inorg. Chem.*, 2015, **54**, 5930.
- 28 K. Katoh, T. Kajiwara, M. Nakano, Y. Nakazawa, W. Wernsdorfer, N. Ishikawa, B. K. Breedlove, M. Yamashita, *Chem. Eur. J.*, 2011, **17**, 117.
- 29 M.-X. Yao, Q. Zheng, K. Qian, Y. Song, S. Gao, J.-L. Zuo, *Chem. Eur. J.*, 2013, **19**, 294.
- 30 (a) V. Chandrasekhar, S. Hossain, S. Das, S. Biswas, J.-P. Sutter, *Inorg. Chem.*, 2013, **52**, 6346. (b) R. J. Blagg, F. Tuna, E. J. L. McInnes, R. E. P. Winpenny, *Chem. Commun.*, 2011, **47**, 10587.
- 31 (a) S. Titos-Padilla, J. Ruiz, J. M. Herrera, E. K. Brechin, W. Wernsdorfer, F. Lloret, E. Colacio, *Inorg. Chem.*, 2013, **52**, 9620. (b) R. J. Blagg, L. Ungur, F. Tuna, J. Speak, P. Comar, D. Collison, W. Wernsdorfer, E. J. McInnes, L. F. Chibotaru, R. E. Winpenny, *Nat. Chem.*, 2013, **5**, 673.

Table 1 Crystal Data and Structure Refinement for **1–3**

	1	2	3
Empirical formula	C ₇₂ H ₈₄ GdN ₃ NiO ₉ S ₄	C ₇₂ H ₈₄ TbN ₃ NiO ₉ S ₄	C ₇₂ H ₈₄ DyN ₃ NiO ₉ S ₄
Formula weight	1479.62	1481.29	1484.87
Crystal system	Triclinic	Triclinic	Triclinic
Space group	<i>P</i> $\bar{1}$	<i>P</i> $\bar{1}$	<i>P</i> $\bar{1}$
<i>a</i> (Å)	11.7413(8)	11.7563(15)	11.7432(11)
<i>b</i> (Å)	17.4898(11)	17.521(2)	17.4859(17)
<i>c</i> (Å)	18.9005(12)	18.887(2)	18.8642(18)
α (°)	72.1160(10)	72.230(2)	72.2850(10)
β (°)	79.3280	79.386(2)	79.4140(10)
γ (°)	77.7270	77.672(2)	77.774(2)
<i>V</i> (Å ³)	3579.2(4)	3589.5(8)	3576.5(6)
ρ calc (g/cm ³)	1.373	1.371	1.379
<i>F</i> (000)	1530	1532	1534
data / restraints / parameters	13136 / 0 / 829	13282 / 0 / 829	13242 / 0 / 829
GOF on <i>F</i> ²	1.110	1.027	1.063
<i>R</i> ₁ ^a / <i>wR</i> ₂ ^b [<i>I</i> > 2σ(<i>I</i>)]	0.0433 / 0.1227	0.0473 / 0.1226	0.0367 / 0.1032
<i>R</i> ₁ / <i>wR</i> ₂ [all data]	0.0518 / 0.1426	0.0676 / 0.1487	0.0417 / 0.1094

$$^a R_1 = \frac{\sum ||F_o| - |F_c||}{\sum |F_o|}, \quad ^b wR_2 = \left[\frac{\sum w(F_o^2 - F_c^2)^2}{\sum w(F_o^2)^2} \right]^{0.5}.$$

Table 2 Selected bond lengths (Å) and Ln \cdots Ni distances (Å) for **1–3**

	1 (Gd)	2 (Tb)	3 (Dy)
Ln(1)-O(1)	2.366(3)	2.363(4)	2.350(2)
Ln(1)-O(3)	2.337(3)	2.323(4)	2.297(3)
Ln(1)-O(4)	2.554(3)	2.550(4)	2.547(2)
Ln(1)-O(5)	2.174(3)	2.161(4)	2.148(2)
Ln(1)-O(6)	2.595(3)	2.589(4)	2.580(3)
Ln(1)-O(7)	2.177(3)	2.165(4)	2.157(3)
Ln(1)-O(8)	2.420(3)	2.408(4)	2.398(3)
Ni(1)-O(1)	2.070(3)	2.066(4)	2.070(3)
Ni(1)-O(2)	2.047(3)	2.048(4)	2.045(3)
Ni(1)-O(3)	2.075(3)	2.062(4)	2.077(3)
Ni(1)-N(1)	2.032(4)	2.022(5)	2.040(3)
Ni(1)-N(2)	2.032(4)	2.039(5)	2.034(3)
Ni(1)-N(3)	2.078(4)	2.093(5)	2.087(3)
Ln(1) \cdots Ni(1)	3.4712(6)	3.4568(8)	3.4489(6)

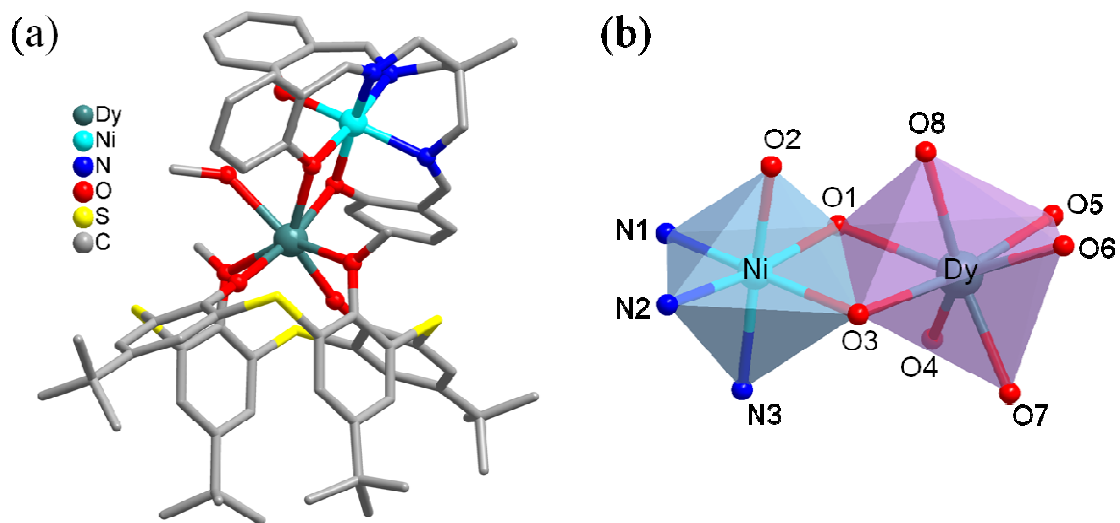


Fig. 1 (a) Crystal structure of complex $[(\text{NiL}_1)\text{Dy}(\text{L}_2)(\text{CH}_3\text{OH})]\cdot\text{acetone}$ (**3**). Hydrogen atoms and uncoordinated solvents are omitted for clarity. (b) Local coordination geometries of Ni^{II} and Dy^{III} ions.

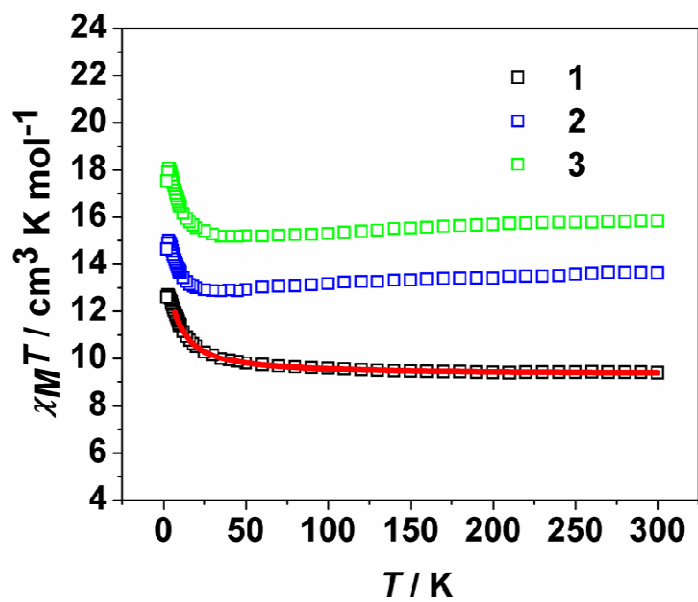


Fig. 2 Temperature dependence of the $\chi_{\text{M}}T$ values for **1–3** in a 1 kOe field.

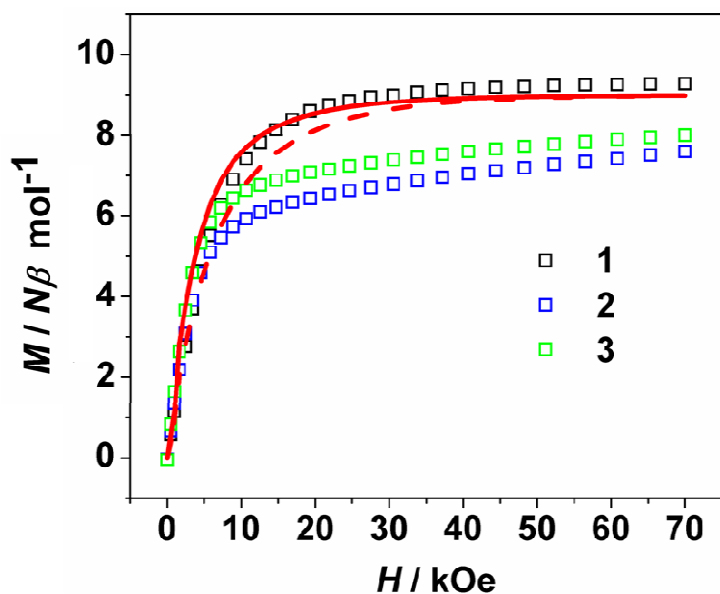


Fig. 3 Field-dependent magnetizations for 1–3 from 0 to 70 kOe at 1.9 K. The red lines represent the Brillouin function, which correspond to the $S = 9/2$ (solid line) and non-interacting $S = S_{\text{Ni}} + S_{\text{Gd}}$ (dashed line) states with $g = 2.05$.

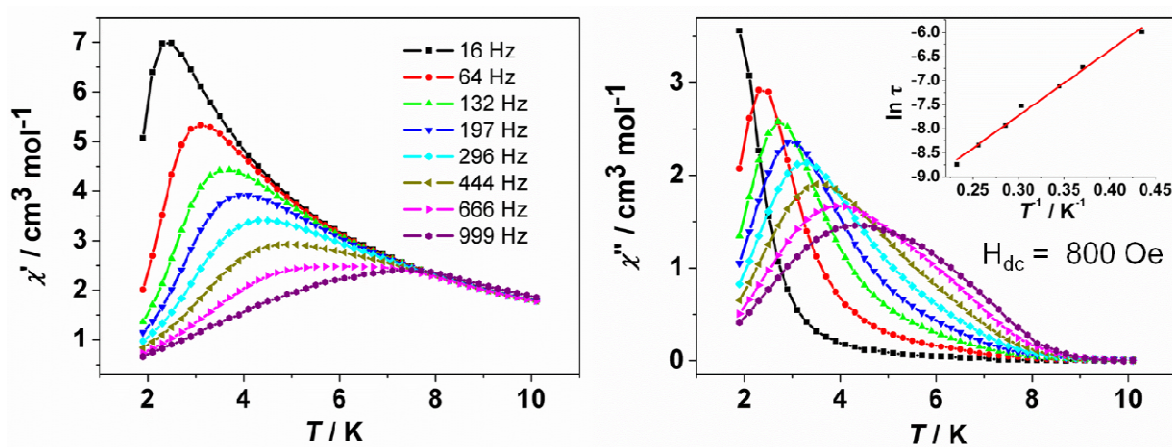


Fig. 4 Temperature-dependent in-phase χ' and out-of-phase χ'' ac susceptibility signals for 3 at the indicated frequencies under 800 Oe dc field. The inset is the Arrhenius fit for the $\ln \tau$ vs. T^{-1} plot.

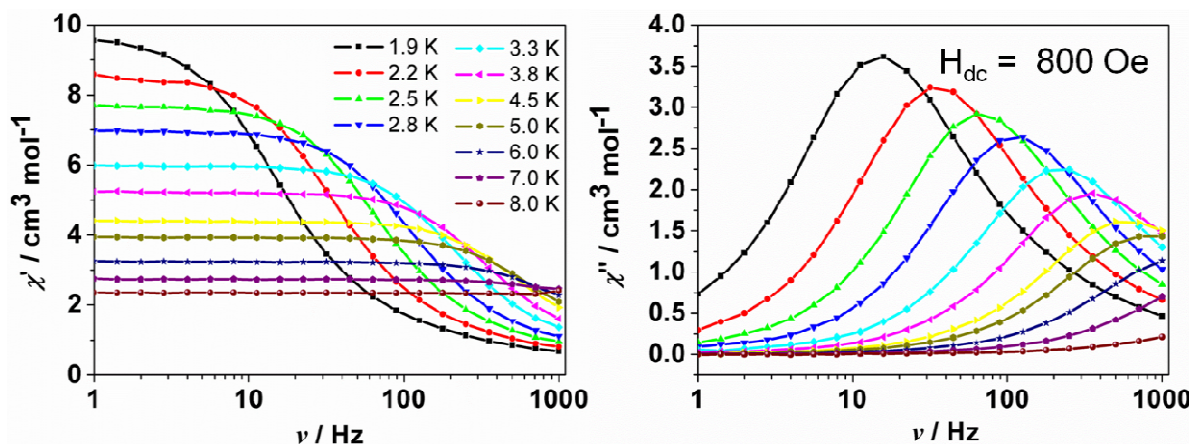


Fig. 5 Frequency-dependent in-phase χ' and out-of-phase χ'' ac susceptibility signals for **3** at the indicated frequencies under 800 Oe dc field.

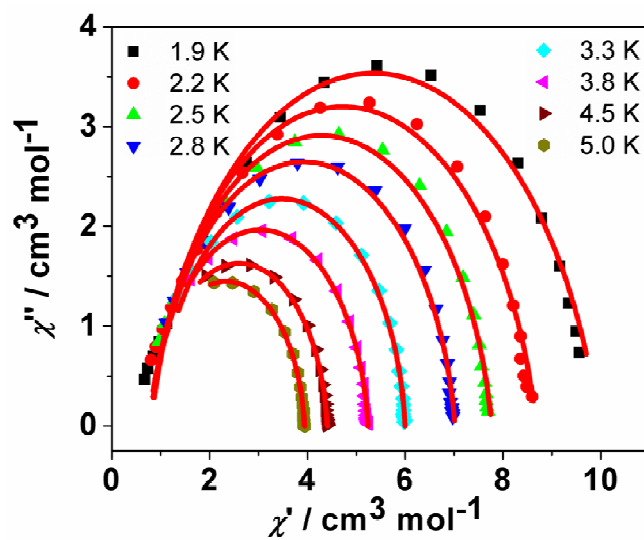


Fig. 6 Cole-Cole plots for **3** under 800 Oe dc field. The solid lines represent the fit to the Debye model at the indicated temperatures.

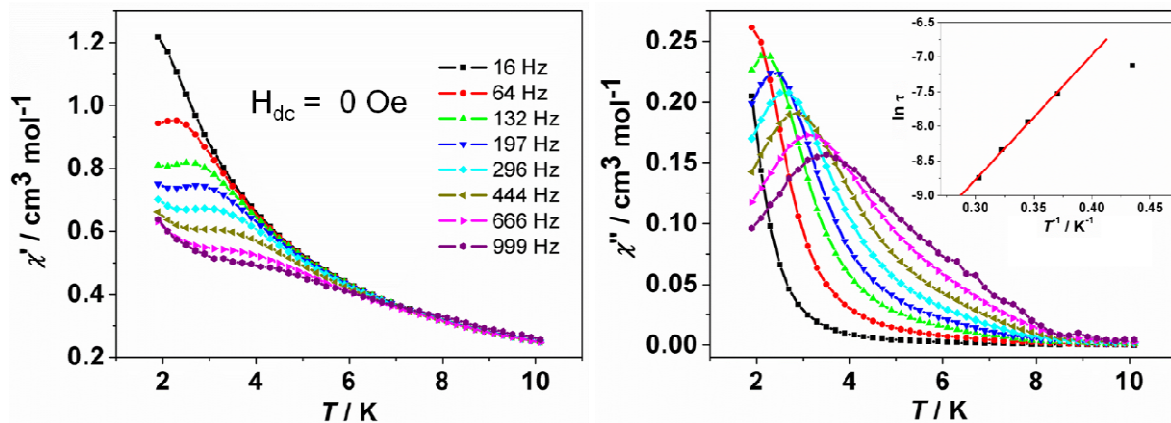


Fig. 7 Temperature-dependent in-phase χ' and out-of-phase χ'' ac susceptibility signals for **3'** at the indicated frequencies under zero dc field. The inset is the Arrhenius fit for the $\ln \tau$ vs. T^{-1} plot.

Graphic Abstract

Three Ni^{II}-Ln^{III} heterodinuclears have been isolated by the method of stepwise synthesis based on thiacalix[4]arene, which is of interest for synthetic inorganic chemistry. Ln^{III} and Ni^{II} ions are doubly bridged by two phenoxo O atoms. Ferromagnetic couplings are operative between the Ni^{II} and Ln^{III} ions. The Dysprosium analogue exhibits the field-induced single-molecule magnet behavior and diamagnetic dilution can efficiently influence the dipole–dipole interaction between magnetic centers.

